Multiphase Simulation of Transport Phenomena During Solidification Processes

Andreas Ludwig and Menghuai Wu
Department of Ferrous Metallurgy, University of Leoben
Franz-Josef Str. 18, A-8700 Leoben, Austria
Tel: +43-(0)3842-402 411, Fax: +43-(0)3842-402 611, Email: ludwig@unileoebn.ac.at

Phase transport phenomena such as melt convection, sedimentation and phase separation play very important role in solidification and structure formation. A two phase volume averaging model is developed. Simulation results demonstrate that this two phase model is able to simulate solidification including nucleation, grain evolution, phase transport, solute transport, macrosegregation etc. The phase transport phenomena lead to macrosegregation, and strongly influence the grain structure distribution. Evaluation efforts were made by comparing the numerical predictions with the experiments. The numerically predicted grain size distribution in a plate casting (Al-4wt%Cu) is found to agree reasonably with the experimental analyses. These encouraging results stimulate further studies and improvements on this model.

Industry casting practice and laboratory investigations have both since long demonstrated the importance of phase transport phenomena such as melt convection, sedimentation or phase separation etc. in solidification, structure and macrosegregation formations[1-3]. However, only recently it is possible to model the solidification process with consideration of these complicated transport phenomena[4-5]. A new and promising model is the volume-averaging approach developed by Beckermann's group[5-11], in which the solidification is considered for the first time as a multiphase and multiscale problem. This approach was further modified by Ludwig et al[12-13]. For globular equiaxed solidification, and some uncertainties appearing in the pioneering model[14-15] handling the complicated dendritic solidification morphology were avoided. This model was recently applied to study globular equiaxed solidification in industry alloys like Al-4wt%Cu and phase separation in hypermonotectic alloys like Al-10wt%Bi. The morphology of the solidified (or decomposed) primary phase was handled as sphere.

In order to briefly describe the basic considerations of the volume-averaging approach developed in literature[12-13], we consider a volume element as schematically shown in **Fig.1.** Convection and sedimentation occur as the primary phase nucleates and grows in the melt. The movement of the solid phase influences the grain structure distribution obviously. Due to solute partitioning at the liquid-solid interface, the average liquid concentration c_l is different from the average solid concentration c_s, the relative movement between the liquid and the solid causes the macrosegregation. In the two phase model considered in this report both liquid phase and secondary phase (solid or second liquid) are treated as separated but coupled and interpenetrating continua. The mass transport equations for both phases are written as

$$\frac{\partial}{\partial t}(f_l\rho_l)+\nabla\cdot(f_l\rho_l\vec{u}_l)=M_{sl} \tag{1}$$

$$\frac{\partial}{\partial t}(f_s\rho_s)+\nabla\cdot(f_s\rho_s\vec{u}_s)=M_{ls}. \tag{2}$$

where f_l, f_s are the volume fraction of the liquid and solid phases, ρ_l, ρ_s are the densities. The liquid is transported according to $\vec{u}_l$, and the solid according to $\vec{u}_s$. The momentum, enthalpy and species conservation equations which are used to determine the other dependent variables such as temperatures T_l, T_s, velocities $\vec{u}_l$, $\vec{u}_s$ and species concentrations c_l, c_s are described elsewhere[5, 12-13, 16]. Interactions between the two phases like mass transfer, friction and drag, solute partitioning and release of latent heat are included in the corresponding exchange and source terms. For example, the $M_{ls}(=-M_{sl})$ in Eq. (1-2) is the mass transfer rate.

The grains are also assumed to be transported according to $\vec{u}_s$. This is taken into consideration by the grain density conservation equation

$$\frac{\partial}{\partial t}n+\nabla\cdot(\vec{u}_s n)=N \tag{3}$$

with grain density *n*, and nucleation rate *N*. Here an empirical 3-parameter nucleation law[4] is used. With the known *n* and f_s, the averaged grain size is estimated $d_s=\sqrt[3]{6f_s/(\pi n)}$.

As an example to demonstrate the capability of the recent model we present simulation results of an Al-4wt%Cu ingot casting in **Fig.2.** With Ti as grain finer, the solidification morphology of this alloy is assumed to be globular. The metallic die at a constant temperature (290 K) is assumed to be filled instantaneously with melt (925 K). The heat exchange coefficient at the casting-mold interface is taken to be 750 W/(m^2.K). An open thermally isolated boundary

condition at the casting top is applied, so that hot melt can feed the casting constantly. The nucleation parameters[4] are taken to be $n_{max}=10^{14}$ m^{-3}, $\Delta T_N=10$ K, $\Delta T_\sigma=4$ K. Constant densities for both liquid and solid are used, hence the thermal-solutal convection is ignored here. The phase transport phenomena in this model consider only solid sedimentation, sedimentation induced melt convection, and feeding flow ($\rho_s > \rho_l$). Further details of the problem description and thermal physical properties used are presented in literature[12-13, 16].

In the initial stage, **Fig. 2** a), feeding flow caused by solidification shrinkage dominants. Nucleation and solidification start first in the four corners, and subsequently along the mold walls. The grains nucleated directly on the wall does not move. With further solidification the grains which are not directly adhered to the mold wall sink downwards, **Fig. 2** b). As the solid and the liquid are coupled through the momentum exchange terms the melt is drawn by the sinking grains, forming two vortices: one clockwise in the right half and one anticlockwise in the left half of the casting. Obviously at this stage of solidification the sedimentation and the sedimentation induced melt convection dominant. Grain settlement occurs as the local f_s exceeds the packing limit $f_s^c \approx 64\%$. The grain movement leads to the accumulation of solid phase in the lower corner and bottom regions. The grain settlement is responsible for the negative segregation in these areas (zones **A** and **D** in **Fig. 2** b-c)). Mechanisms for positive segregations are: (i) feeding of packed zones by segregated melt and (ii) squeezing out of segregated melt by settling grains[16]. The positive segregation zones **B** are caused by the first mechanism, while the zones **C** are caused by the second. The zones **C** occur in the bulk melt. They move with the flow current and ascend towards the inner regions of the casting. As shown in **Fig. 2** c), the grain size distribution along the casting walls is relatively uniform (~ 50 μm). Relative large grains appear in the casting central region. The solid velocity field indicates that these large grains may have been transported from other regions. The grains nucleated along the vertical walls sink and grow. As they reach the lower central regions, they have grown to a relatively large size. As solidification proceeds the zone of large grains moves upwards, while the grains continue to grow.

Fig. 3 shows the simulated solidification process of a hypermonotectic alloy (Al-10wt%Bi) under zero gravity condition. The two phase model used is similar to that for the globular equiaxed solidification. The minority liquid phase (Bi), decomposed from the parent melt as droplets in the miscibility gap, is treated as the second phase L_2, while the parent melt as the first phase L_1. The morphology of the decomposed second phase is assumed to be ideally spherical. The thermocapillary (Marangoni) motion of the second phase droplets is modeled by considering an additional source term, i.e. volume averaged Marangoni force $\bar{F}_M$, in the momentum conservation equations[17]. The thermocapillary force on a single droplet was solved analytically by Young et al[18-20]. The thermocapillary forces acting on all the droplets were integrated and then averaged over the volume element to get the source term $\bar{F}_M$. The monotectic reaction is modeled by adding the latent heat to the first phase L_1 and applying an artificially enlarged viscosity to the solidified monotectic matrix in order to model its drastically reduced flowability on solidification. To test the recent model a simple 2D square casting is simulated. The mold is assumed to remain at a constant temperature (290 K). The heat exchange coefficient at casting-mold interface is taken to be 750 W/(m^2.K).

The nucleation parameters[4] are taken as $n_{max}= 10^{13}$ m^{-3}, $\Delta T_N = 20$ K, $\Delta T_\sigma = 8$ K. For other thermal physical properties we refer to literature[3, 21-23]. As shown in **Fig. 3**, phase separation occurs even without gravity. The only mechanism which causes this phase transport is Marangoni motion. Droplets of L_2 start to nucleate and grow at the casting surface as the local temperature drops below the binodal. The temperature gradient causes the movement of L_2 droplets from surface region towards the casting center. The parent melt moves in reverse direction, because the space of the leaving phase L_2 must be filled by the parent melt L_1. The movement of L_2 from the corners and from the surface regions towards the casting center will result in a decrease of L_2 volume fraction f_2 in the corners and surface regions and an increase in the casting center. As the casting further cools down to the monotectic point, the monotectic reaction occurs. Thus, the velocity of L_1 vanishes and the L_2 droplets are entrapped in the monotectic matrix. Final solidification results show that the amount of L_2 phase is low in the surface region and high in the inner region. Phase separation is directly responsible for the macrosegregation. Both Marangoni motion and diffusion controlled growth contribute to the uneven droplet size distribution. A tendency of finer droplets in the surface regions and relatively large droplets in the central region is predicted.

At present we are working further on this model to include (1) the free surface formed at the casting top or the concentrated pores in the casting due to the solidification shrinkage; (2) the thermal-solutal convection; (3) the reliable nucleation and grain growth parameters; (4) the collision and coagulation, which are important in hypermonotectic solidification; (5) the parallel computing technique to extend the calculation from 2D to 3D; etc.

Despite of the model assumptions which need further improvements, evaluation efforts were made by comparing the numerical predictions with a special experimental situation. **Fig. 4** shows the simulated grain size distribution in a section of an Al-4wt%Cu plate casting, compared with the experimental results. The globular equiaxed model, mentioned above, was used for the simulations. The mold temperature was taken to be 573 K and the heat exchange coefficient at casting-mold interface to be 800 W/(m^2.K). An convection heat exchange boundary condition on the top surface of the casting was applied, the convection heat transfer coefficient was taken as 50 W/(m^2.K) and the environmental temperature as 283 K. The solidification shrinkage and the thermal-solutal convection are ignored for this case, but sedimentation and sedimentation induced convection were considered with the Boussinesq approach. Sedimentation and sedimentation induced flow currents, similar to the results shown in **Fig. 2**, are also observed in the considered cross section of the plate casting: two vortices occur - one clockwise in the right part and one anticlockwise in the left part of the section. The numerically predicted grain size distribution cross the section of the plate casting is shown in **Fig. 4** a). The fine grain size (~262 μm) at the bottom region is mainly due to the high nucleation rate in the initial stage, and partially due to the sedimentation. The largest grains (~390 μm) are predicted near the surface regions about 30~40 mm above the bottom. Those large grains are actually transported from the upper regions. They nucleate in the upper region. They sink and grow. As they reach lower regions through a relatively long journey, they have grown to a large size. The relatively small grains predicted in the central region are due to the melt currents, which transport the fine grains from bottom regions upwards to the center. As compared in **Fig. 4** b) and c), the grain size distribution in the real casting agree

reasonably with the numerical prediction. The absolute values for the grain sizes are somehow different between the numerical simulation and the experiment, but the distribution pattern is quite similar. The casting section is also EDX (energy dispersive X-ray) analyzed for macrosegregation. The experimentally measured data are relatively scatter. It is difficult to fit the experimental data to the numerical results quantitatively. However, the measured result shows the same tendency as the simulation. There is a lower concentration in casting bottom region and a higher concentration in top region. Considering the simplifications made in the present model, we find the above agreement between the simulation and the experiment encouraging.

It is claimed that the present model approach can be further developed as tool to simulate the solidification process including nucleation, grain evolution, melt convection, sedimentation, phase separation, macro structure and segregation formation etc.

Acknowledgement

This work was financially *supported* by the German Science Foundation (DFG) as part of the collaborative research centers "Integral Materials Modeling", the ESA-MAP project "Solidification Morphologies of Monotectic Alloys-MONOPHAS" and the DLR project "Simulation of the Dynamics of Monotectic Solidification".

Literature

[1] A. Ohno, Solidification - *The separation theory and its practical applications*, Springer-Verlag, Berlin, **1987**.
[2] J. Campbell, *Castings*, Butterworth Heinemann Ltd, Oxford, **1991**.
[3] L. Ratke und S. Diefenbach, *Mater. Sci. Eng.* **1995**, *15(R)*, 263-347.
[4] M. Rappaz, *Int. Mater. Rev.* **1989**, *34*, 93-123.
[5] C. Beckermann and R. Viskanta, *Appl. Mech. Rev.* **1993**, *46*, 1-27.
[6] J. Ni and C. Beckermann, *Metall. Trans.* B **1991**, *22*B, 349-361.
[7] C.Y. Wang and C. Beckermann, *Metall. Mater. Trans.* A **1996**, *27*A, 2754-2764.
[8] C.Y. Wang and C. Beckermann, *Metall. Mater. Trans.* A **1996**, *27*A, 2765-2783.
[9] C.Y. Wang and C. Beckermann, *Metall. Mater. Trans.* A **1996**, *27*A, 2784-2795.
[10] C. Beckermann, *JOM* **1997**, *49*, 13-17.
[11] A.V. Reddy and C. Beckermann, *Metall. Mater. Trans.* B **1997**, *28*B, 479-489.
[12] A. Ludwig, G. Ehlen, M. Pelzer and P.R. Sahm PR, *Proc. MCWASP IX, SIM2000*, Aachen, Shaker-Verlag, **2000**, 175-182.
[13] A. Ludwig, M. Wu, G. Ehlen and P.R. Sahm, *Materials Week 2000*, Sept. 25-28, **2000**, Munich, Germany.
[14] J. Ni and F.P. Incropera, *Inter. J. Heat Mass Transfer* **1995**, *38*, 1271-1284.
[15] J. Ni and F.P. Incropera, *Inter. J. Heat Mass Transfer* **1995**, *38*, 1285-1296.
[16] A. Ludwig and M. Wu, *Metall. Mater. Trans.* A **2002**, *33*, 3673-3683.
[17] M. Wu, A. Ludwig and L. Ratke, accepted by *McWASP X*, Destin, Florida, May 25-30, **2003**.
[18] N.O. Young, J.S. Goldstein and M.J. Block, *J. Fluid Mech.* **1959**, 6, 350-356.
[19] W. Günter, *Über die Dynamik von Fluidpartikeln aufgrung des Marangoni-Effektes*, Düsseldorf, VDI-Verlag, **1993**.
[20] M.G. Velarde, in L. Ratke, H. Walter, B. Feuerbacher (eds.), *Materials and Fluids under Low Gravity*, Springer Berlin, **1995**, 283-298.
[21] S. Diefenbach, *Modellierung der Gefügeentwicklung von Monotekta*, Thesis, Ruhr-University Bochum, **1993**.
[22] F. Falk, in L. Ratke (eds.), *Immiscible Liquid Metals and Organics* **1993**, DGM Informationsgesellschaft mbH, 93-100.
[23] L. Ratke, S. Dree, S. Diefenbach, B. Pronz and A. Ahlborn, in L. Ratke, H. Walter, B. Feuerbacher (Eds.), *Materials and Fluids under Low Gravity* **1995**, Springer Berlin, 115-133.

Figures

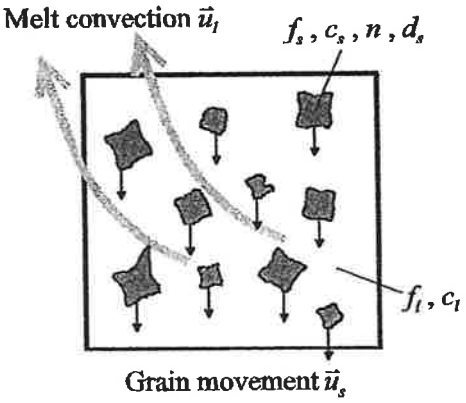

Fig. 1: Schematic drawing of the melt convection and grain movement in a volume element.

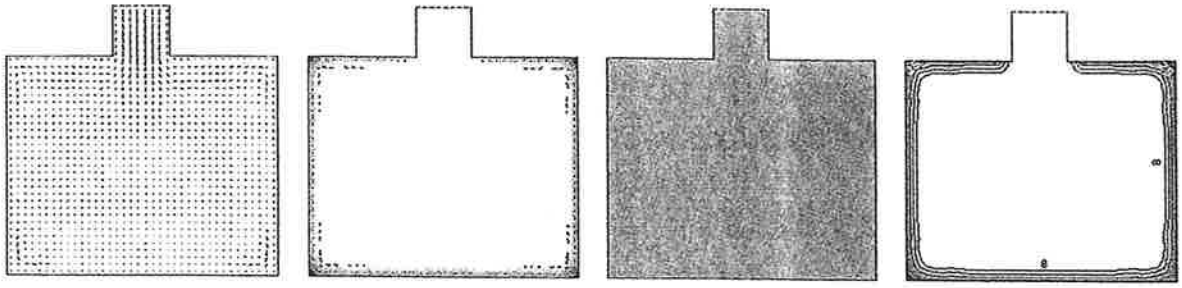

$\vec{u}_{l,\max} = 0.47$ mm/s $\quad \vec{u}_{s,\max} = 0.39$ mm/s, $\quad C_{mix\,(wt\%)}$ $\quad d_{s\,(\mu m)}$

f_s in gray scale 0~0.64

a) 5 s after cooling starts

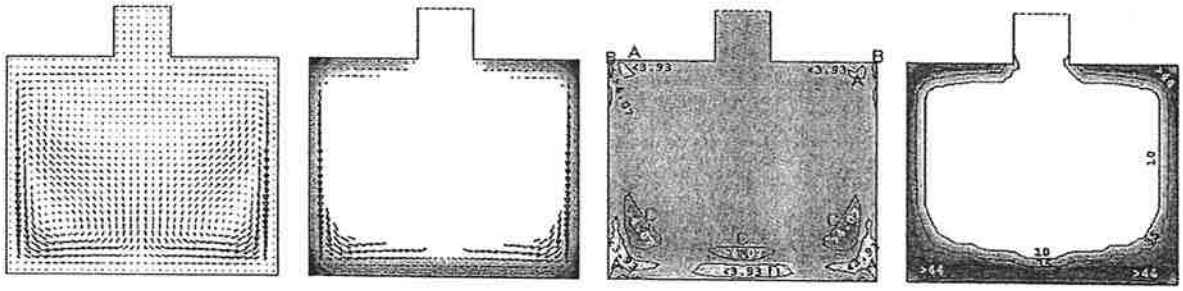

$\vec{u}_{l,\max} = 21$ mm/s $\quad \vec{u}_{s,\max} = 21$ mm/s, $\quad C_{mix\,(wt\%)}$ $\quad d_{s\,(\mu m)}$

f_s in gray scale 0~0.86

b) 16 s after cooling starts

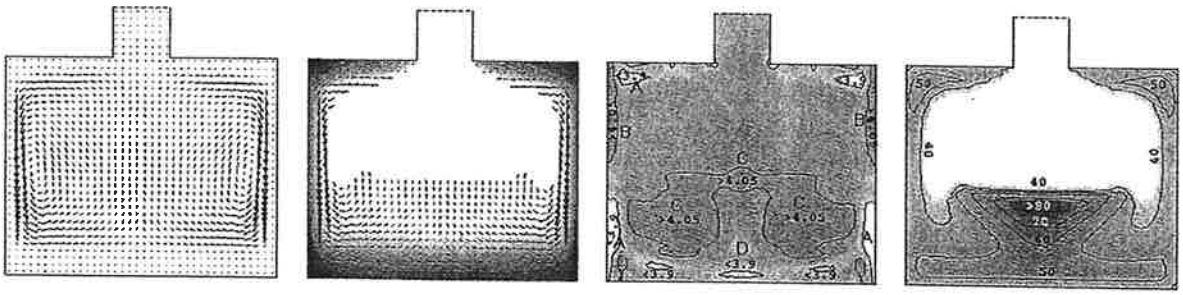

$\vec{u}_{l,\max} = 30$ mm/s $\quad \vec{u}_{s,\max} = 30$ mm/s, $\quad C_{mix\,(wt\%)}$ $\quad d_{s\,(\mu m)}$

f_s in gray scale 0~0.92

c) 28 s after cooling starts

Fig. 2: Solidification process of a 180x150 mm^2 Al-4wt%Cu ingot casting. The arrows of both velocities are linearly scaled from zero to the maximum value given. The fraction solid f_s is shown together with the solid velocity. c_{mix} and d_s are shown with isolines together with 30 gray levels, with dark showing the highest value and bright the lowest.

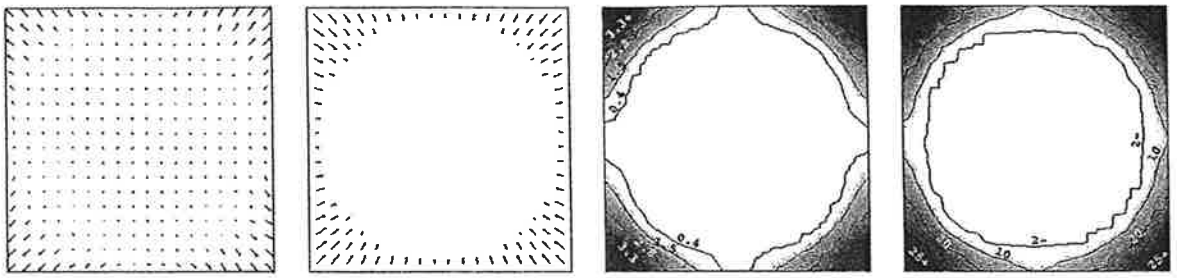

$\vec{u}_{1,max} = 0.018$ mm·s^{-1} $\vec{u}_{2,max} = 0.44$ mm·s^{-1} f_2 (%) d_2 (µm)

a) 3.6 s after cooling starts

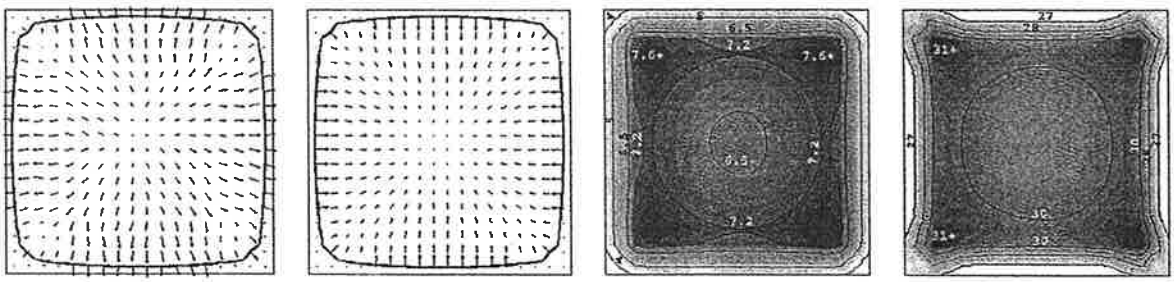

$\vec{u}_{1,max} = 0.011$ mm·s^{-1} $\vec{u}_{2,max} = 0.21$ mm·s^{-1} f_2 (%) d_2 (µm)

b) 15.6 s after cooling starts

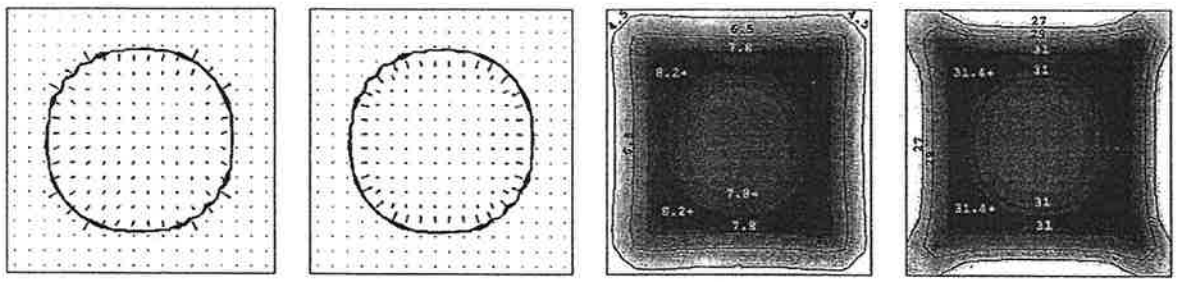

$\vec{u}_{1,max} = 0.016$ mm·s^{-1} $\vec{u}_{2,max} = 0.16$ mm·s^{-1} f_2 (%) d_2 (µm)

c) 32.6 s after cooling starts

Fig. 3: Solidification process of a 90x90 mm^2 square casting with a hypermonotectic alloy Al-10wt%Bi under zero gravity conditions. The arrows of both velocities are linearly scaled from zero to the maximum value given. The monotectic reaction front (T=930 K) is also drawn together with the velocity field. All other quantities are shown with isolines together with 30 gray levels, with dark showing the highest value and bright the lowest.

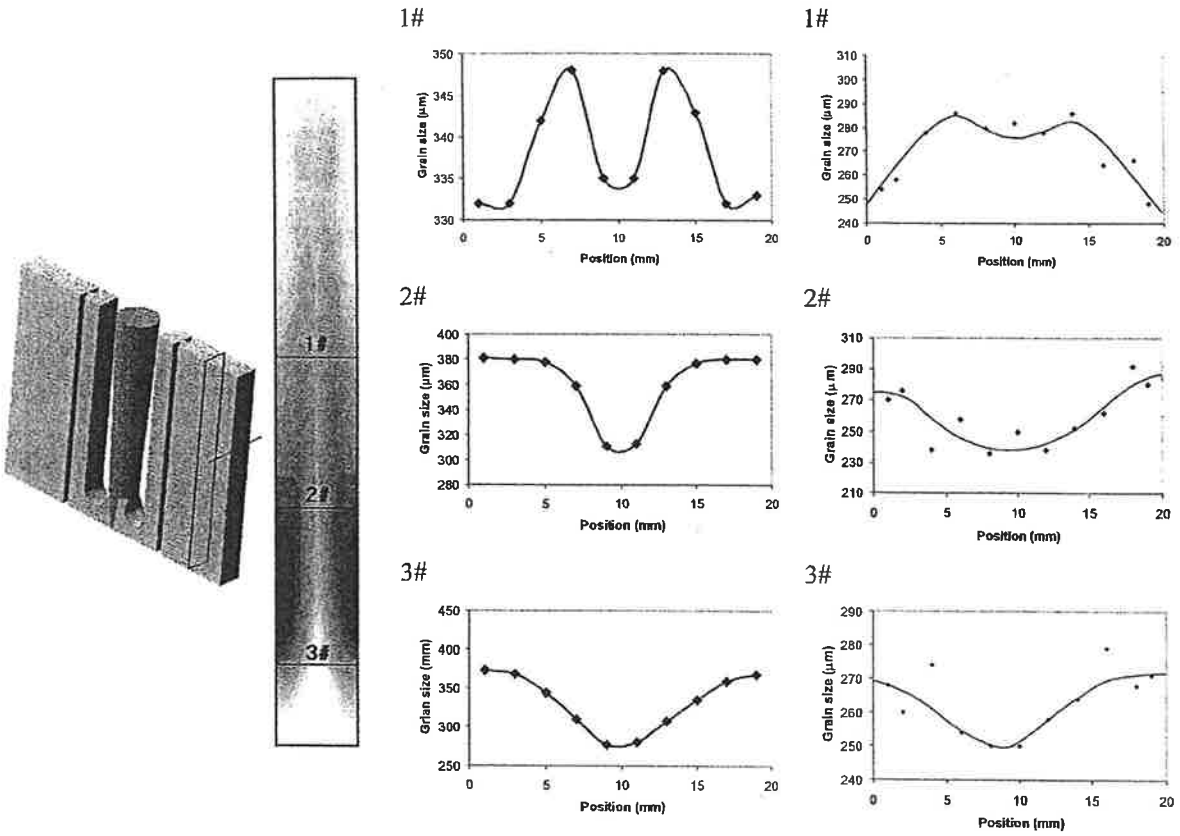

a) Simulation is made in a vertical section of the casting. The grain size distribution is shown with 30 gray levels, with light showing the smallest grains (262 μm), and dark the largest (390 μm).

b) Simulated grain size distribution across the considered section at 3 different positions 1#, 2# and 3#.

c) The experimental casting is sectioned, and the grain size distribution at the corresponding positions 1#, 2# and 3# are metallographically analyzed.

Fig. 4: Comparison of the numerically predicted grain size distribution in an Al-4wt%Cu plate casting to the experimentally measured results. The nucleation parameters[4] for simulation are $n_{max}= 1.5 \cdot 10^{12}$ m^{-3}, $\Delta T_N = 20$ K, $\Delta T_\sigma = 8$ K.